

Comparison of Filtering Algorithms for Ground Target Tracking Using Space-based GMTI Radar

M. Mallick¹, B. La Scala², B. Ristic³, T. Kirubarajan⁴, and J. Hill⁵

¹Independent Consultant, Anacortes, WA, USA, mahendra.mallick@gmail.com

²National Australia Bank, Melbourne, Australia, Barbara.F.La.Scala@nab.com.au

³DSTO, Port Melbourne, branko.ristic@dsto.defence.gov.au

⁴McMaster University, Hamilton, ON, Canada, kiruba@mcmaster.ca

⁵Vencore, Chantilly, VA, USA, Joe.hill@vencore.com

Abstract—Space-based radar (SBR) systems have received a great deal of attention, since they can provide all-weather, day-night, and continuous world-wide surveillance and tracking of ground, air, and sea-surface targets. The ground moving target indicator (GMTI) mode is an important operating mode for such systems. GMTI radar measurements are the range, azimuth and range-rate, which are nonlinear functions of the target state. We consider the extended Kalman filter (EKF), unscented Kalman filter (UKF), and particle filter (PF) for the SBR GMTI nonlinear filtering problem and present a new track initiation algorithm. We compare the mean square errors (MSEs) and computational times using simulated data generated by Monte Carlo simulations. Although the cross-range errors are large, our results show that the MSEs of the filters are nearly the same. Our results show that the EKF performs the best for the scenario considered based on the MSE and computational time.

Keywords: Space-based Radar, Ground Target Tracking, Nonlinear Filtering, GMTI Filtering.

I. INTRODUCTION

A radar-based surveillance system offers all-weather and day-night surveillance which is not possible for an optical or infrared (IR) based surveillance system. Moreover, a space-based radar (SBR) system has significant advantages over a ground-based or airborne radar system for providing continuous and world-wide observation, surveillance, and tracking of ground, air, and sea-surface targets. Therefore, SBR systems have drawn a great deal of interest in recent years [4]–[6], [18], [20]. A snapshot of the orbit of a space-based sensor is shown in Figure 1.

Typical SBR systems consist of a constellation of radar satellites in low- or medium-altitude Earth orbits and associated ground-based support systems. Such systems have a number of operating modes which include the ground moving target indicator (GMTI) for land, littoral and maritime targets, open ocean surveillance (OOS), medium and high-resolution synthetic aperture radar (SAR), high resolution terrain information (HRTI), and advanced geospatial intelligence (AGI). An important area of research is that of designing effective strategies for switching between operating modes in order to best achieve the mission objectives [6], [20].

A key prerequisite for optimal mode switching is that the system operates efficiently in each individual mode. In



Figure 1. STK screenshot of orbit with 45 degree FOV conical sensor ground projection.

this paper, we concentrate on ground target tracking using measurements from a SBR in the GMTI mode. In this mode, the radar uses the range-rate or Doppler measurements to distinguish moving target returns from clutter.

Published work in open literature on SBR filtering or tracking is limited. In [21], the authors address filtering using the interacting multiple model (IMM) estimator [3], where each single-mode filter is an extended Kalman filter (EKF) [1], [3], [8]. The Earth relative spherical polar coordinates and their first time derivative are used to define as the state in [21]. In this paper, we focus on selecting an appropriate filtering algorithm for a target moving on the plane tangent to the WGS 84 reference ellipsoid [14] using space-based GMTI radar measurements. The filtering problem is nonlinear due to the nonlinear measurement model. We consider the commonly used approximate nonlinear filtering algorithms; the EKF [1], [3], [8], unscented Kalman filter (UKF) [10], [22], and particle filter (PF) [2], [7], [9], [19]. Previous studies have shown that the widely used EKF performs poorly for certain nonlinear filtering problems and the UKF and PF perform better than the EKF [19]. Therefore, the UKF and PF have drawn a great deal of interest in recent years for solving nonlinear filtering problems. The UKF and PF use

the deterministic sampling (quasi-Monte Carlo) and random (Monte Carlo) sampling, respectively. The computational time of the UKF is comparable to that of the EKF. However, the computational time of the PF is significantly higher due to the use of Monte Carlo sampling. The UKF and PF do not necessarily provide more accurate solutions than the EKF for all nonlinear filtering problems. For example, for the bearing-only filtering problem [19], the EKF diverges in certain cases and the PF works robustly in all scenarios and provides better tracking accuracy than the EKF [19]. On the contrary, the performance of the EKF, UKF, and PF for the ground moving target filtering problem using an airborne standoff GMTI radar sensor are comparable to each other [12].

The standard deviations for range, azimuth, and range-rate of a GMTI radar sensor are a few meters, milli-radians, and meters per second respectively. Therefore, a SBR GMTI radar provides good localization along the range direction. However, since the distance between the target and GMTI sensor can be hundreds to thousands of kilometers, the cross-range error is large. Thus, the EKF may perform poorly due to linearization used in the nonlinear measurement model. In contrast, as the UKF and PF do not use linearization in the measurement model, they may prove to be more robust. In this paper, we test these hypotheses by considering the filtering problem of a single ground moving target using a space-based GMTI radar in a low-earth orbit.

The outline of the paper is as follows. In Section II we describe various coordinate frames and define conventions used. Sections III and IV present the target dynamic model and measurement model for the SBR GMTI sensor. Section V describes a new track initiation algorithm using the first GMTI measurement while Section VI summarizes the EKF, UKF, and transition density-based PF (TD-PF) filtering algorithms. Finally, Sections VII and VIII present numerical results and conclusions.

II. COORDINATE FRAMES AND CONVENTIONS

We use the symbol “:=” to define a quantity and \mathbf{A}' denotes the transpose of the vector or matrix \mathbf{A} . The measurement model and track initiation use a number of coordinate frames and transformations of physical 3-vectors among coordinate frames. We assume that all coordinate frames are right-handed and orthogonal. An uppercase roman letter (e.g. \mathbf{A}) is used to denote the coordinate frame \mathbf{A} . We use $\mathbf{b} \in \mathbb{R}^3$ and $\mathbf{b}^{\mathbf{A}} \in \mathbb{R}^3$ to represent a physical 3-vector in a coordinate-free representation and in the \mathbf{A} frame, respectively, where $(b_x^{\mathbf{A}}, b_y^{\mathbf{A}}, b_z^{\mathbf{A}})$ represent the Cartesian components of $\mathbf{b}^{\mathbf{A}}$ along the $X, Y,$ and Z axes of the \mathbf{A} frame. Let $\mathbf{b}^{\mathbf{B}}$ represent \mathbf{b} in the \mathbf{B} frame. Then the transformation of $\mathbf{b}^{\mathbf{A}}$ to $\mathbf{b}^{\mathbf{B}}$ is described by $\mathbf{b}^{\mathbf{B}} = \mathbf{T}_{\mathbf{A}}^{\mathbf{B}} \mathbf{b}^{\mathbf{A}}$, where $\mathbf{T}_{\mathbf{A}}^{\mathbf{B}}$ is a 3×3 rotational transformation matrix representing the passive rotation from the \mathbf{A} frame to the \mathbf{B} frame. Note, $\mathbf{T}_{\mathbf{A}}^{\mathbf{B}}$ is orthogonal, i.e. $(\mathbf{T}_{\mathbf{A}}^{\mathbf{B}})^{-1} = (\mathbf{T}_{\mathbf{A}}^{\mathbf{B}})' = \mathbf{T}_{\mathbf{B}}^{\mathbf{A}}$.

Next, we describe the coordinate frames.

- 1) WGS 84 Earth-centered Earth-fixed coordinate frame (E frame) – The origin of the E frame is at the center of

mass of the Earth. The Z axis is along the Earth’s axis of rotation. The X axis is directed from the center of the Earth to the intersection of the Greenwich meridian and the equator. The Y axis completes the right-handed coordinate frame.

- 2) Tracker coordinate frame (T frame) – Let $\lambda_0, \phi_0,$ and $h_0 = 0$ denote the geodetic longitude, latitude, and height of the T frame origin. The T frame is a topographic coordinate frame at $(\lambda_0, \phi_0, 0)$ for which the $X, Y,$ and Z axes are along the local East, North, and upward direction, respectively.
- 3) Sensor local coordinate frame (L frame) – Let $\lambda_s, \phi_s,$ and h_s denote the geodetic longitude, latitude, and height of the sensor. The origin of the L frame is at $(\lambda_s, \phi_s, 0)$. The L frame is a topographic coordinate frame at $(\lambda_s, \phi_s, 0)$ for which the $X, Y,$ and Z axes are along the local East, North, and upward direction, respectively.

The relationship between the T frame and the E frame is illustrated in Figure 2.

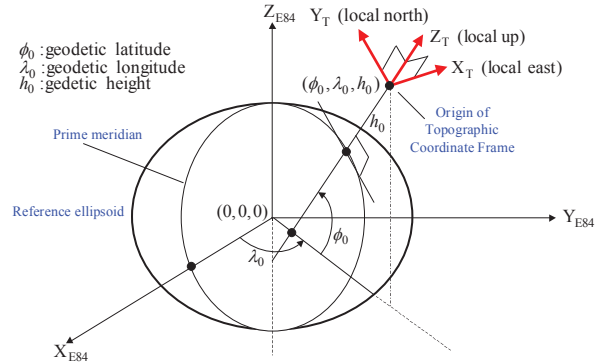


Figure 2. Topographic coordinate frame (T frame) and Earth-centered Earth-fixed WGS 84 (E frame) coordinate frames.

III. TARGET DYNAMIC MODEL

We assume that the target moves in the XY plane of the T frame with the nearly constant velocity (NCV) motion [3]. Let (x_k, y_k) and (\dot{x}_k, \dot{y}_k) denote the position and velocity of the target at time t_k . Then the target state $\mathbf{x}_k \in \mathbb{R}^4$ at time t_k is defined by

$$\mathbf{x}_k := [x_k \quad y_k \quad \dot{x}_k \quad \dot{y}_k]' \quad (1)$$

The dynamic model is given by

$$\mathbf{x}_k = \mathbf{F}_{k,k-1} \mathbf{x}_{k-1} + \mathbf{w}_{k,k-1}, \quad (2)$$

where $\mathbf{F}_{k,k-1}$ is the state transition matrix [3], [8] and $\mathbf{w}_{k,k-1}$ is a zero-mean white Gaussian integrated process noise [3],

[8] with covariance $\mathbf{Q}_{k,k-1}$. For the NCV motion, $\mathbf{F}_{k,k-1}$ and $\mathbf{Q}_{k,k-1}$ are given by [3]

$$\mathbf{F}_{k,k-1} := \begin{bmatrix} 1 & 0 & \Delta_k & 0 \\ 0 & 1 & 0 & \Delta_k \\ 0 & 0 & 1 & 0 \\ 0 & 0 & 0 & 1 \end{bmatrix}, \quad (3)$$

$$\mathbf{Q}_{k,k-1} := \begin{bmatrix} q_1 \Delta_k^3/3 & 0 & q_1 \Delta_k^2/2 & 0 \\ 0 & q_2 \Delta_k^3/3 & 0 & q_2 \Delta_k^2/2 \\ q_1 \Delta_k^2/2 & 0 & q_1 \Delta_k & 0 \\ 0 & q_2 \Delta_k^2/2 & 0 & q_2 \Delta_k \end{bmatrix}, \quad (4)$$

where $\Delta_k := t_k - t_{k-1}$ and q_1 and q_2 are the power spectral densities of the white noise acceleration process noise along the X and Y axes respectively.

IV. SPACE-BASED RADAR GMTI MEASUREMENT MODEL

A. Measurement Model

Define

- $\mathbf{p}^T \in \mathbb{R}^3$: Cartesian components of the target 3D position vector from the T frame origin expressed in the T frame,
- $\mathbf{v}^T \in \mathbb{R}^3$: Cartesian components of the target 3D velocity relative to the T frame expressed in the T frame,
- $\mathbf{p}_s^T \in \mathbb{R}^3$: Cartesian components of the sensor 3D position vector from the T frame origin expressed in the T frame,
- $\mathbf{v}_s^T \in \mathbb{R}^3$: Cartesian components of the sensor 3D velocity relative to the T frame expressed in the T frame.

Let

$$\mathbf{p}^T := [x \ y \ z]^T = [x \ y \ 0]^T, \quad (5)$$

$$\mathbf{v}^T := [\dot{x} \ \dot{y} \ \dot{z}]^T = [\dot{x} \ \dot{y} \ 0]^T, \quad (6)$$

$$\mathbf{p}_s^T := [x_s \ y_s \ z_s]^T, \quad (7)$$

$$\mathbf{v}_s^T := [\dot{x}_s \ \dot{y}_s \ \dot{z}_s]^T. \quad (8)$$

The state of the sensor is defined by

$$\mathbf{x}^s := [(\mathbf{p}_s^T)' \ (\mathbf{v}_s^T)']^T. \quad (9)$$

Let $\mathbf{r}^T \in \mathbb{R}^3$ denote the range vector from the sensor to the target expressed in the T frame,

$$\mathbf{r}^T := \mathbf{p}^T - \mathbf{p}_s^T. \quad (10)$$

Dropping the time index for clarity, the nonlinear GMTI measurement model is given by

$$\mathbf{z} = \mathbf{h}(\mathbf{x}, \mathbf{x}_s) + \mathbf{n}, \quad (11)$$

where \mathbf{z} is the GMTI measurement with components range, azimuth, and range-rate and \mathbf{h} is the nonlinear measurement function. We assume that the measurement noise \mathbf{n} is zero-mean white and Gaussian with a diagonal covariance \mathbf{R}

$$\mathbf{R} := \text{diag}(\sigma_r^2, \sigma_\alpha^2, \sigma_{\dot{r}}^2), \quad (12)$$

where σ_r^2 , σ_α^2 , and $\sigma_{\dot{r}}^2$ are the measurement error variances for range, azimuth, and range-rate, respectively. The measurement function for range is

$$h_r(\cdot, \cdot) = r := [(\mathbf{r}^T)' \mathbf{r}^T]^{1/2}. \quad (13)$$

The measurement function for the azimuth angle is defined in the L frame and is given by [14]

$$h_\alpha(\cdot, \cdot) = \alpha := \begin{cases} \tan^{-1}(r_x^L, r_y^L), & \text{if } \tan^{-1}(r_x^L, r_y^L) > 0, \\ \tan^{-1}(r_x^L, r_y^L) + 2\pi, & \text{otherwise,} \end{cases} \quad (14)$$

where $\mathbf{r}^L = \mathbf{T}_T^L \mathbf{r}^T$. We calculate \mathbf{T}_T^L by

$$\mathbf{T}_T^L = \mathbf{T}_E^L(\lambda_s, \phi_s) [\mathbf{T}_E^T(\lambda_0, \phi_0)]', \quad (15)$$

where

$$\mathbf{T}_E^T(\lambda_0, \phi_0) = \mathbf{G}(\lambda_0, \phi_0), \quad (16)$$

$$\mathbf{T}_E^L(\lambda_s, \phi_s) = \mathbf{G}(\lambda_s, \phi_s), \quad (17)$$

$$\mathbf{G}(\lambda, \phi) := \begin{bmatrix} -\sin \lambda & \cos \lambda & 0 \\ -\sin \phi \cos \lambda & -\sin \phi \sin \lambda & \cos \phi \\ \cos \phi \cos \lambda & \cos \phi \sin \lambda & \sin \phi \end{bmatrix}. \quad (18)$$

The measurement function for range-rate is

$$h_{\dot{r}}(\cdot, \cdot) = \dot{r} := (\dot{\mathbf{r}}^T)' \mathbf{u}^T, \quad (19)$$

where

$$\dot{\mathbf{r}}^T := \mathbf{v}^T - \mathbf{v}_s^T = [\dot{r}_x^T \ \dot{r}_y^T \ \dot{r}_z^T]', \quad (20)$$

and \mathbf{u}^T is a unit vector in the direction of \mathbf{r}^T ,

$$\mathbf{u}^T := \frac{\mathbf{r}^T}{r} = [u_x^T \ u_y^T \ u_z^T]'. \quad (21)$$

B. Jacobian Matrix

Let \mathbf{H} denote the derivative of the measurement function \mathbf{h} with respect to the target state

$$\mathbf{H}(\mathbf{x}, \mathbf{x}^s) := \frac{\partial \mathbf{h}(\mathbf{x}, \mathbf{x}^s)}{\partial \mathbf{x}}. \quad (22)$$

It can be shown that the only non-zero elements of \mathbf{H} are given by

$$H_{11} = u_x^T, \quad H_{1,2} = u_y^T, \quad (23)$$

$$H_{21} = \frac{1}{\rho} (\mathbf{T}_T^L(1,1)r_y^L - \mathbf{T}_T^L(2,1)r_x^L), \quad (24)$$

$$H_{22} = \frac{1}{\rho} (\mathbf{T}_T^L(1,2)r_y^L - \mathbf{T}_T^L(2,2)r_x^L), \quad (25)$$

$$H_{31} = \frac{1}{r} (\dot{r}_x^T - \dot{r} u_x^T), \quad (26)$$

$$H_{32} = \frac{1}{r} (\dot{r}_y^T - \dot{r} u_y^T), \quad (27)$$

$$H_{33} = u_x^T, \quad H_{34} = u_y^T, \quad (28)$$

where $\rho = (r_x^L)^2 + (r_y^L)^2$.

V. TRACK INITIATION ALGORITHM

Tracking is done in the T frame, whereas the azimuth angle is defined in the L frame for a GMTI radar [14]. Most published papers consider these two frames as the same [16]. When this is the case, track initiation is straightforward. However, when the distance between the target and the sensor is large, as in the case of a stand-off GMTI radar or space-based GMTI radar, then the difference between these two frames can have significant effect on the angle measurement

model (azimuth, elevation) and track initiation. Here we present a new track initiation algorithm using the SBR GMTI measurement.

First we assume that we have error-free range r and azimuth α GMTI measurements. Let δ denote the depression angle of the range-vector \mathbf{r} . The depression angle is the angle between the range vector and a plane parallel to the horizontal plane at the sensor location and is unknown. Next we present an algorithm for determining δ . Since r, α , and δ define \mathbf{r} in the L frame, we have

$$\mathbf{r}^L = r \begin{bmatrix} \cos \delta \sin \alpha & \cos \delta \cos \alpha & -\sin \delta \end{bmatrix}', \quad (29)$$

where $\delta > 0$ and

$$\mathbf{r}^T = \mathbf{T}_L^T \mathbf{r}^L. \quad (30)$$

Using the above equation for \mathbf{r}^T and (10), we get

$$\mathbf{p}^T = \mathbf{p}_s^T + \mathbf{T}_L^T \mathbf{r}^L. \quad (31)$$

The Z component of (31) gives

$$z = z_s + \mathbf{T}_L^T(3, 1)r_x^L + \mathbf{T}_L^T(3, 2)r_y^L + \mathbf{T}_L^T(3, 3)r_z^L. \quad (32)$$

Since by definition (5), $z = 0$, we have

$$z_s + \mathbf{T}_L^T(3, 1)r_x^L + \mathbf{T}_L^T(3, 2)r_y^L + \mathbf{T}_L^T(3, 3)r_z^L = 0. \quad (33)$$

Use of (29) in (33) and rearrangement of terms yield

$$\begin{aligned} z_s + r \cos \delta [\mathbf{T}_L^T(3, 1) \sin \alpha + \mathbf{T}_L^T(3, 2) \cos \alpha] \\ = r \mathbf{T}_L^T(3, 3) \sin \delta. \end{aligned} \quad (34)$$

Define

$$\beta_1 := -z_s, \quad (35)$$

$$\beta_2 := r \mathbf{T}_L^T(3, 3), \quad (36)$$

$$\beta_3 := r [\mathbf{T}_L^T(3, 1) \sin \alpha + \mathbf{T}_L^T(3, 2) \cos \alpha]. \quad (37)$$

Then we can write (34) as

$$\beta_1 + \beta_2 \sin \delta = \beta_3 \cos \delta. \quad (38)$$

Squaring both sides of (38) and simplifying, we get

$$\sin^2 \delta + b_1 \sin \delta + b_2 = 0, \quad (39)$$

where

$$b_1 := \frac{2\beta_1\beta_2}{(\beta_2^2 - \beta_3^2)}, \quad b_2 := \frac{(\beta_1^2 - \beta_3^2)}{(\beta_2^2 - \beta_3^2)}. \quad (40)$$

Two solutions exist for $\sin \delta$. However, since $\delta > 0$, the only acceptable solution is

$$\delta = \sin^{-1}[-b_1 + (b_1^2 - 4b_2)^{1/2}], \quad \delta > 0. \quad (41)$$

Now, suppose we have GMTI measurements (z_r, z_α, z_r) . We assume that the sensor position is error-free¹. Then the X and Y components of target position estimates in the T frame are calculated using (31) and (29) by setting $r = z_r$

¹We shall consider errors in sensor position and velocity in our future work.

and $\alpha = z_\alpha$. The initial 3D position estimate of the target in the T frame is given by

$$\hat{\mathbf{p}}^T = \mathbf{p}_s^T + \mathbf{T}_L^T \hat{\mathbf{r}}^L. \quad (42)$$

Let $\hat{\mathbf{x}}_{1|1}$ denote the initial state estimate by using the first GMTI range and azimuth measurements. The X and Y velocity components of $\hat{\mathbf{x}}_{1|1}$ are set to zero. Then

$$\hat{\mathbf{x}}_{1|1} = \begin{bmatrix} \hat{p}_x^T & \hat{p}_y^T & 0 & 0 \end{bmatrix}'. \quad (43)$$

The error in the estimated target position $\hat{\mathbf{p}}^T$ is given by

$$\hat{\mathbf{p}}^T = \mathbf{p}_s^T + \mathbf{T}_L^T \tilde{\mathbf{r}}^L, \quad (44)$$

where

$$\tilde{\mathbf{r}}^L = \mathbf{T}_L^T \mathbf{A} \begin{bmatrix} \tilde{r} & \tilde{\alpha} \end{bmatrix}', \quad (45)$$

and

$$\mathbf{A} := \begin{bmatrix} \cos \delta \sin \alpha & r \cos \delta \cos \alpha \\ \cos \delta \cos \alpha & -r \cos \delta \sin \alpha \\ -\sin \delta & 0 \end{bmatrix}. \quad (46)$$

In deriving (45), we have neglected the error in δ . Let $\mathbf{P}_{\hat{\mathbf{p}}}^T$ denote the covariance associated with $\hat{\mathbf{p}}^T$. Then

$$\mathbf{P}_{\hat{\mathbf{p}}}^T := \mathbb{E} [\tilde{\mathbf{p}}^T (\tilde{\mathbf{p}}^T)'] = \mathbf{T}_L^T \mathbf{A} \mathbf{R}_{r\alpha} \mathbf{A}' (\mathbf{T}_L^T)', \quad (47)$$

where $\mathbf{R}_{r\alpha} := \text{diag}(\sigma_r^2, \sigma_\alpha^2)$. Let \mathbf{P}_0^T denote the 2×2 matrix corresponding to the XY components of $\mathbf{P}_{\hat{\mathbf{p}}}^T$. Then the covariance matrix corresponding to $\hat{\mathbf{x}}_{1|1}$ is given by

$$\mathbf{P}_{1|1} = \begin{bmatrix} \mathbf{P}_0^T & \mathbf{0}_{2 \times 2} \\ \mathbf{0}_{2 \times 2} & \left(\frac{v_{\max}^2}{3} \right) \mathbf{I}_2 \end{bmatrix}, \quad (48)$$

where v_{\max} is the maximum possible speed of a ground target. Now, $\hat{\mathbf{x}}_{1|1}$ and $\mathbf{P}_{1|1}$ are based on the first range and azimuth measurements and associated variances. Next, $\hat{\mathbf{x}}_{1|1}$ and $\mathbf{P}_{1|1}$ are updated by processing the first range-rate measurement with an EKF.

VI. SBR GMTI NONLINEAR FILTERING ALGORITHMS

The dynamic and measurement models for the SBR GMTI filtering problem are linear (2) and nonlinear (11), respectively. The prediction and update steps for the EKF, UKF, and PF are described next.

A. Extended Kalman Filter

The extended Kalman filter is an extension of the Kalman filter to a nonlinear filtering problem. For the current scenario, the nonlinear measurement model is linearized about the predicted state estimate and then the Kalman filter algorithm is applied [3], [8]. It generally works well provided the degree of nonlinearity (DoN) [15] of the measurement function is not high and the error in the initial state estimate is sufficiently small [11]. If these conditions are not satisfied then the filter will diverge.

The predicted state estimate, $\hat{\mathbf{x}}_{k|k-1}$, and the corresponding error covariance matrix, $\mathbf{P}_{k|k-1}$, are given by the *prediction* step [1], [3]

$$\hat{\mathbf{x}}_{k|k-1} = \mathbf{F}_{k,k-1} \hat{\mathbf{x}}_{k-1|k-1}, \quad (49)$$

$$\mathbf{P}_{k|k-1} = \mathbf{F}_{k,k-1} \mathbf{P}_{k-1|k-1} \mathbf{F}'_{k,k-1} + \mathbf{Q}_{k,k-1}. \quad (50)$$

The predicted measurement is [3], [8]

$$\hat{\mathbf{z}}_{k|k-1} = \mathbf{h}_k(\hat{\mathbf{x}}_{k|k-1}). \quad (51)$$

The measurement updated state estimate, $\hat{\mathbf{x}}_{k|k}$, and the corresponding error covariance, $\mathbf{P}_{k|k}$, are given by the *update* step [1], [3]

$$\hat{\mathbf{x}}_{k|k} = \hat{\mathbf{x}}_{k|k-1} + \mathbf{K}_k(\mathbf{z}_k - \hat{\mathbf{z}}_{k|k-1}), \quad (52)$$

$$\mathbf{P}_{k|k} = \mathbf{P}_{k|k-1} - \mathbf{K}_k \mathbf{S}_k \mathbf{K}'_k, \quad (53)$$

where the Kalman gain is

$$\mathbf{K}_k = \mathbf{P}_{k|k-1} \mathbf{H}'_k \mathbf{S}_k^{-1}, \quad (54)$$

and the innovation covariance is

$$\mathbf{S}_k = \mathbf{H}_k \mathbf{P}_{k|k-1} \mathbf{H}'_k + \mathbf{R}_k. \quad (55)$$

B. Unscented Kalman Filter

Unlike the EKF, the unscented Kalman filter [10], [22] does not approximate the nonlinearities in the system. Instead, it approximates the posterior density of the state estimates using a Gaussian distribution. For this system, as the state dynamics are linear, the predicted state estimate $\hat{\mathbf{x}}_{k|k-1}$, predicted error covariance $\mathbf{P}_{k|k-1}$, updated state estimate $\hat{\mathbf{x}}_{k|k}$, and the updated error covariance, $\mathbf{P}_{k|k}$ are still given by (49), (50), (52), and (53), respectively. However, the predicted measurement, gain matrix, and innovation covariance are computed differently.

The UKF of [22] uses different weights for the mean $\{w_m^j\}_{j=0}^{2n}$ and covariance $\{w_c^j\}_{j=0}^{2n}$ which are given by

$$w_m^0 = \frac{\lambda}{(n + \lambda)}, \quad (56)$$

$$w_c^0 = \frac{\lambda}{(n + \lambda) + (1 - \alpha^2 + \beta)}, \quad (57)$$

and

$$w_c^m = w_c^j = \frac{1}{2(n + \lambda)}, \quad (58)$$

for $j = 1, \dots, 2n$, where $\lambda = \alpha^2(n + \kappa) - n$ is a scaling parameter. The parameter α determines the spread of the sigma points around the conditional mean $\hat{\mathbf{x}}_{k|k}$ and is set to a small positive value (e.g. 1e-3). The parameter β is a secondary scaling parameter and is usually set to zero and β used to incorporate prior knowledge of the distribution of \mathbf{x} and for Gaussian distributions the optimal value of β is two. The weights are constant for all measurement times.

Given $\hat{\mathbf{x}}_{k-1|k-1}$ and $\mathbf{P}_{k-1|k-1}$, the UKF calculates the sigma points $\{\hat{\mathbf{x}}_{k|k}^j\}_{j=0}^{2n}$

$$\hat{\mathbf{x}}_{k-1|k-1}^0 = \hat{\mathbf{x}}_{k-1|k-1}, \quad (59)$$

$$\hat{\mathbf{x}}_{k-1|k-1}^j = \hat{\mathbf{x}}_{k-1|k-1} + \left(\sqrt{(n + \lambda) \mathbf{P}_{k-1|k-1}} \right)_j, \quad (60)$$

for $j = 1, \dots, n$ and

$$\hat{\mathbf{x}}_{k-1|k-1}^j = \hat{\mathbf{x}}_{k-1|k-1} - \left(\sqrt{(n + \lambda) \mathbf{P}_{k-1|k-1}} \right)_j, \quad (61)$$

for $j = n + 1, \dots, 2n$, where $(\sqrt{(n + \lambda) \mathbf{P}_{k-1|k-1}})_j$ is the j^{th} column of the matrix square root.

The predicted measurement is given by

$$\hat{\mathbf{z}}_{k|k-1} \approx \sum_{j=0}^{2n} w_m^j \mathbf{z}_{k|k-1}^j, \quad (62)$$

where

$$\mathbf{z}_{k|k-1}^j := \mathbf{h}(\mathbf{x}_{k|k-1}^j, \mathbf{x}_k^s). \quad (63)$$

The gain \mathbf{K}_k and innovation covariance \mathbf{S}_k are given by

$$\mathbf{K}_k := \Psi_k \mathbf{S}_k^{-1}, \quad (64)$$

$$\mathbf{S}_k \approx \mathbf{R}_k + \sum_{j=0}^{2n} w_c^j (\mathbf{z}_{k|k-1}^j - \hat{\mathbf{z}}_{k|k-1})(\mathbf{z}_{k|k-1}^j - \hat{\mathbf{z}}_{k|k-1})', \quad (65)$$

$$\Psi_k \approx \sum_{j=0}^{2n} w_c^j (\mathbf{x}_{k|k-1}^j - \hat{\mathbf{x}}_{k|k-1})(\mathbf{z}_{k|k-1}^j - \hat{\mathbf{z}}_{k|k-1})'. \quad (66)$$

C. Particle Filter

In contrast to the unscented Kalman filter, particle filter based approaches do not make any assumptions about the distribution of the state. Instead, they seek a set of particles $\{\mathbf{x}_k^i\}$ and weights $\{w_k^i\}$ such that

$$p(\mathbf{x}_k | \mathbf{Z}^k) \approx \sum_{i=1}^N w_k^i \mathbf{x}_k^i, \quad (67)$$

where N is the number of particles and \mathbf{Z}^k represents all the measurements up to and including time t_k . Good overview of the use of particle filters for target tracking can be found in [7], [19].

In this paper we use a variant of the particle filter approach known as the transition density based particle filter (TD-PF) [2], [17], [19]. Given a prior density for the initial state $p_0(\mathbf{x}_1)$, the filter is initialized by generating N particles $\{\mathbf{x}_1^i\}$ from this density. Equal weights are used, $w_1^i = 1/N, i = 1, 2, \dots, N$. At each time t_k , the algorithm then operates as follows:

1) Prediction Step

- Draw N samples $\{\mathbf{x}_k^i\}$ from $p(\mathbf{x}_k | \mathbf{x}_{k-1}^i)$.
- Update the weights using

$$w_k^i = \frac{1}{\gamma} w_{k-1}^i p(\mathbf{z}_k | \mathbf{x}_k^i),$$

where $\gamma = \sum_{i=1}^N w_k^i$ is a normalization constant.

2) Update Step

Compute the updated state estimate and corresponding error covariance matrix using

$$\hat{\mathbf{x}}_{k|k} = \sum_{i=1}^N w_k^i \mathbf{x}_k^i, \quad (68)$$

$$\mathbf{P}_{k|k} = \sum_{i=1}^N w_k^i (\mathbf{x}_k^i - \hat{\mathbf{x}}_{k|k})(\mathbf{x}_k^i - \hat{\mathbf{x}}_{k|k})'. \quad (69)$$

3) Resampling Step

- Compute the effective sample size

$$N_{\text{eff}} = \frac{1}{\sum_{i=1}^N (w_k^i)^2}.$$

- If $N_{\text{eff}} \leq N_{\text{thres}}$ then generate a new set of N particles by resampling, with replacement, from $\{\mathbf{x}_k^i\}$. Reset the weights to $w_k^i = 1/N$.

The final resampling step, and its associated threshold N_{thres} , is required to prevent the filter from degenerating [19].

VII. NUMERICAL SIMULATION AND RESULTS

The goal of this paper is to investigate the robustness, accuracy, and computational times of three common nonlinear filtering algorithms; the EKF, UKF, and PF for ground target tracking using a space-based GMTI radar. A significant source of error in this problem is the large cross-range measurement error and this is the issue we will focus on here. In order to do this, we examine the problem of tracking a single target moving in a plane tangent to the WGS 84 reference ellipsoid with NCV motion. The power spectral densities of the acceleration process noise [3] along the X and Y axes are chosen as equal with a value of $0.5\text{m}^2/\text{s}^3$. The satellite carrying the SBR GMTI sensor moves in a non-precussing circular orbit with a given inclination. Three sets of simulations were carried out using azimuth measurement error standard deviations of 1.0, 2.0, and 3.0 milli-radians. The measurement error standard deviations for range and range-rate were held fixed at 20m and 0.5 m/s, respectively. A sample truth target trajectory and calculated sensor measurement positions with 0.99 probability error ellipses from a single Monte Carlo run are shown in Figure 3. We observe in Figure 3 that the ellipses are long and narrow due to the large cross-range error and small range error. For this scenario, the range is minimum at the midpoint of the trajectory and gradually increases towards the beginning and end of the trajectory. Therefore, the major axes of the error ellipses increase as we move from the midpoint towards the beginning and end of the trajectory. Given the large distance

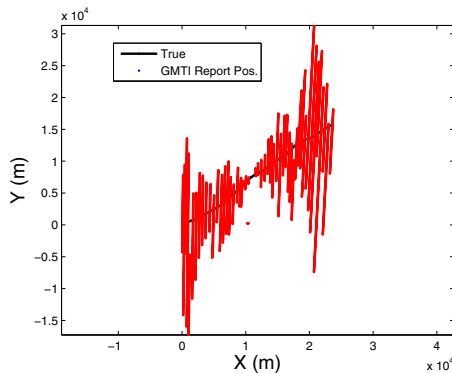


Figure 3. A sample target trajectory in the XY plane and GMTI report locations with 0.99 probability error ellipses. The measurement noise standard deviation for azimuth is 2.0 milli-rad.

from the sensor to the target, these azimuth standard deviations induce significant cross-range errors.

The EKF, UKF, and PF were run on 200 Monte Carlo simulations for each case. We used 1k, 2k, 4k, 6k, 7k, 8k, 10k, and 15k particles for the TD-PF to determine the number of particles that would yield state estimation accuracies that are comparable or better than that of the EKF or UKF. We found that the TD-PF with 10k particles had state estimation accuracy comparable to that of the EKF or UKF. A higher number of particles such as 15k didn't produce a noticeable improvement. The average computational times relative to the EKF are presented in Table I. For each filtering algorithm, the sample trajectory estimates from a single Monte Carlo run are shown in Figure 4, where the TD-PF used 10k particles.

Table I
AVERAGE COMPUTATIONAL TIMES RELATIVE TO THE EKF.

EKF	UKF	TD-PF, 4k	TD-PF, 7k	TD-PF, 10k	TD-PF, 15k
1.0	1.3	36.7	61.4	82.9	136.8

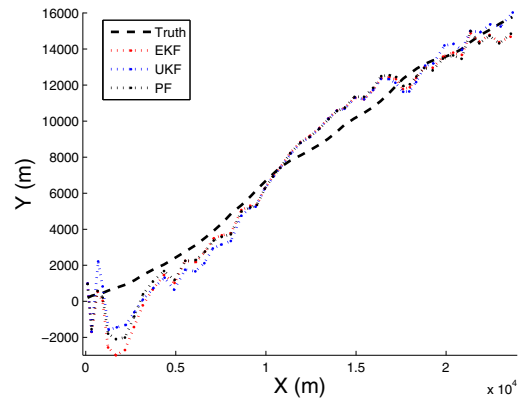


Figure 4. Sample trajectory estimates in the XY plane. The TD-PF used 10k particles. The measurement noise standard deviation for azimuth is 2.0 milli-rad.

Let $\mathbf{x}_{k,m}$ and $\hat{\mathbf{x}}_{k|k,m}$ be the true state and estimated state from the m -th Monte Carlo run respectively and let $\mathbf{P}_{k|k,m}$ be the corresponding error covariance matrix. The following performance metrics were computed to evaluate the performance of each filter,

- bias error,

$$\bar{\mathbf{e}}_k := \frac{1}{M} \sum_{m=1}^M \mathbf{e}_{k,m},$$

where M is the number of Monte Carlo runs and $\mathbf{e}_{k,m}$

is the estimation error, $\mathbf{e}_{k,m} := \mathbf{x}_{k,m} - \hat{\mathbf{x}}_{k|k,m}$,

- the mean square error matrix (MSEM)

$$\text{MSEM}_k := \frac{1}{M} \sum_{m=1}^M \mathbf{e}_{k,m} \mathbf{e}'_{k,m},$$

- the normalized estimation error squared (NEES) [3]

$$\text{NESS}_k := \frac{1}{Mn} \sum_{m=1}^M \mathbf{e}'_{k,m} \mathbf{P}_{k|m}^{-1} \mathbf{e}_{k,m},$$

where n is the dimension of the target state defined in (1). The NEES is a measure of the consistency of the filter calculated covariance. Assuming the errors are normally distributed, the NEES has a Chi-square distribution with one degree of freedom [3]. If the filter calculated covariance is consistent with the estimation error, then NEES would lie within the two-sided 95% confidence bounds most of the time.

The log of the trace of the MSEM for all three filters for the scenario with azimuth standard deviation of 2 milliradians is shown in Figure 5. Figure 6 shows the variation of the log of the trace of the MSEM with 4k, 7k, and 10k particles. The bias errors in the position and velocity estimates are shown in Figure 7 and Figure 8, respectively. These figures show that all three filters provide nearly the same tracking accuracy. Similar pattern is observed for other two scenarios. Based on the tracking accuracy and computational time, we conclude that the EKF is the best candidate for the SBR GMTI filtering scenario considered. These results were contrary to our prior expectation that the EKF may yield poor performance due to the large cross-range error and may diverge in certain cases. Note, all three filters have significant bias due to transients induced by large cross-range errors in the initial track estimates.

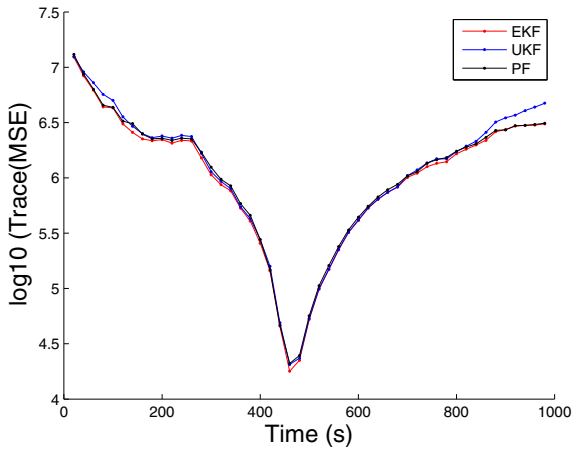


Figure 5. $\log(\text{tr}(\text{MSEM}))$ for the EKF, UKF and PF using the azimuth measurement error standard deviation of 2.0 milli-rad.

Examination of the NEES in Figure 9 indicates the filter-calculated covariance and estimation errors are not consistent at a number of observation times. All three filters suffer from significant track initiation transients. Even after the transient has passed, the UKF and in particular the PF still exceed the limits of the two-sided 95% confidence interval at a number of observation times. The NEES for the PF improves by using 15k particles as shown in Figure 10, but still is not as good as

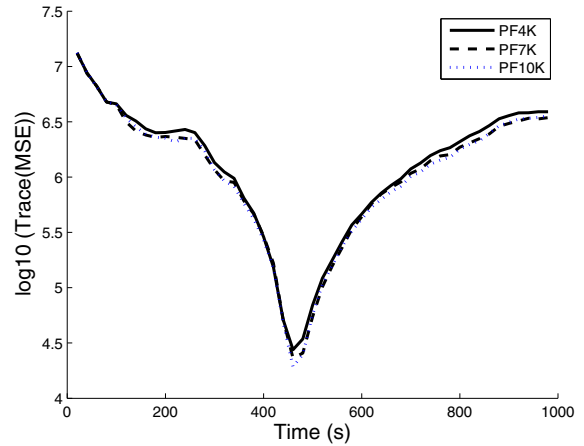


Figure 6. $\log(\text{tr}(\text{MSEM}))$ for the PF with 4k, 7k, and 10k particles using the azimuth measurement error standard deviation of 2.0 milli-rad.

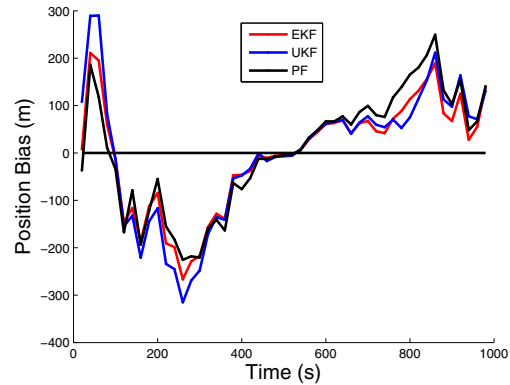


Figure 7. Bias in the position estimates for the EKF, UKF and PF when the azimuth measurement error standard deviation is 2.0 milli-rad.

the NEES from the EKF. Although the log of the trace of the MSEM for the PF with 4k, 7k, and 10k particles in Figure 6 are close to each other, the NEES for the PF with 4k and 7k particles are poor.

VIII. CONCLUSIONS

In this paper we compared the EKF, UKF, and PF for the space-based GMTI nonlinear filtering problem in terms of tracking accuracy, estimation bias, covariance consistency using the NEES and computational time. We used simulated data with Monte Carlo simulations. We presented a new track initiation algorithm using space-based GMTI range, azimuth, and range-rate measurements. This algorithm can be easily extended to a realistic ground target tracking scenario with terrain elevation data.

Our numerical results show that the tracking accuracies of the three nonlinear filters are nearly the same. It is surprising that the EKF performs well in spite of large cross-range

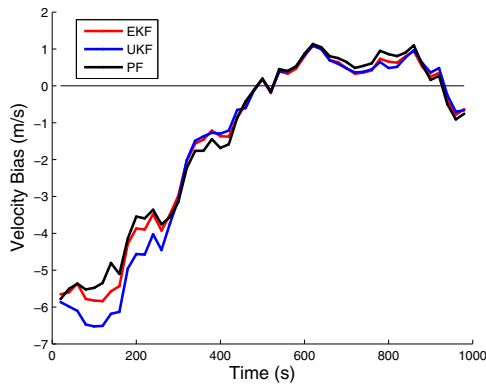


Figure 8. Bias in the velocity estimates for the EKF, UKF and PF when the azimuth measurement error standard deviation is 2.0 milli-rad.

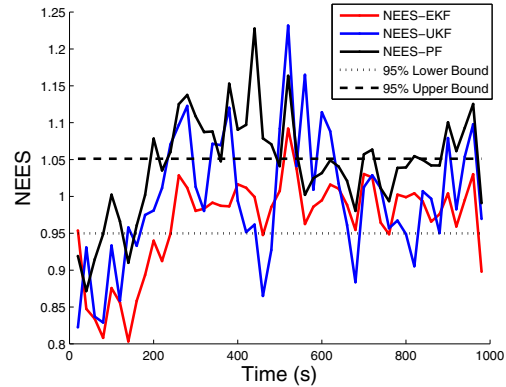


Figure 10. Normalized estimation error squared for all three filters when the azimuth measurement error standard deviation is 2.0 milli-rad.

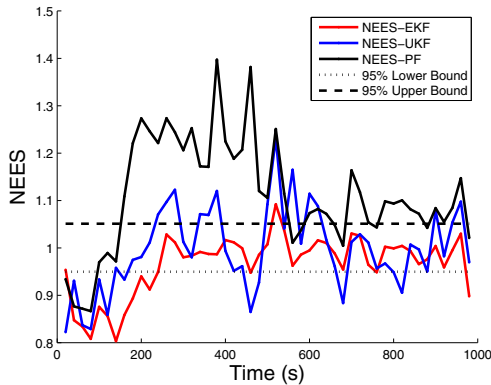


Figure 9. Normalized estimation error squared for all three filters when the azimuth measurement error standard deviation is 2.0 milli-rad.

errors and does not diverge. Our results show that the EKF has the best NEES values among the three filters. Therefore, the EKF is the best candidate algorithm for the space based GMTI filtering scenario considered based on all four metrics. Our future work will focus on improving the track initiation algorithm by using unbiased converted measurements and covariance consistency.

REFERENCES

- [1] B. Anderson and J. Moore, *Optimal Filtering*, Prentice Hall, 1979.
- [2] S. Arulampalam, S. Maskell, N. Gordon, and T. Clapp, "A tutorial on particle filters for on-line non-linear/non-Gaussian Bayesian tracking," *IEEE Transactions on Signal Processing*, vol. 50, no. 2, pp. 174–188, 2002.
- [3] Y. Bar-Shalom, X. R. Li, and T. Kirubarajan, *Estimation with Applications to Tracking and Navigation*, Wiley & Sons, 2001.
- [4] L. J. Cantafio, Ed., *Space-based Radar Handbook*, Artech House, 1989.
- [5] G. R. Curry, "A low-cost space-based radar system concept," *IEEE AES Systems Magazine*, vol. 11, no. 9, pp. 21–24, 1996.
- [6] M. E. Davis, "Space based radar technology challenges," *Proc. IEEE Aerospace Conference*, Big Sky, MT, USA, Mar 2006.
- [7] A. Doucet and A. M. Johansen, "A tutorial on particle filtering and smoothing: Fifteen years later," *Handbook of Nonlinear Filtering*, vol. 12, pp. 656–704, 2009.

- [8] A. Gelb, Ed., *Applied Optimal Estimation*, MIT Press, 1974.
- [9] N. J. Gordon, D. J. Salmund, and A. F. M. Smith, "Novel approach to nonlinear/non-Gaussian Bayesian state estimation," *IEE Proceedings-F*, vol. 140, no. 2, pp. 107–113, April 1993.
- [10] S. J. Julier and J. K. Uhlmann, "Unscented filtering and nonlinear estimation," *Proceedings of the IEEE*, vol. 92, no. 3, pp. 401–422, 2004.
- [11] B. F. La Scala, R. R. Bitmead, and M. R. James, "Conditions for the stability of the extended Kalman filter and their application to the frequency tracking problem," *Mathematics of Control, Signals and Systems*, vol. 8, no. 1, pp. 1–27, 1995.
- [12] M. Mallick and S. Arulampalam, "Comparison of nonlinear filtering algorithms in ground moving target indicator (GMTI) target tracking," *Proc. SPIE Conference on Signal and Data Processing of Small Targets*, vol. 5204, Orlando, FL, USA, 2003.
- [13] M. Mallick, "Comparison of video filtering algorithms," in *Tenth ONR/GTRI Workshop on Target Tracking and Sensor Fusion*, vol. 5204, Monterey, California, USA, May 22–23, 2007.
- [14] —, "Maximum likelihood geolocation using a ground moving target indicator radar," in *IEEE Aerospace Conference*, Big Sky, MT, USA, Mar 2002.
- [15] M. Mallick, B. F. La Scala, and S. Arulampalam, "Differential geometry measures of nonlinearity with applications to target tracking," *Proc. Fred Daum Tribute Conference*, Monterey, CA, USA, May 2007.
- [16] L. Mo, X. Song, Y. Zhou, Z. K. Sun, and Y. Bar-Shalom, "Unbiased converted measurements for tracking," *IEEE Trans. on Aerospace and Electronic Systems*, vol. 34, no. 3, pp. 1023–1027, 1998.
- [17] M. R. Morelande ; S. Challa ; N. J. Gordon, "Application of particle filters to single-target tracking problems," *Proc. SPIE Conference on Signal and Data Processing of Small Targets*, vol. 5204, San Diego, CA, USA, 2003.
- [18] S. U. Pillai, K. Y. Li, and B. Himed, *Space Based Radar: Theory Applications*, McGraw Hill, New York, 2008.
- [19] B. Ristic, S. Arulampalam, and N. Gordon, *Beyond the Kalman Filter*. Artech House, 2004.
- [20] P. A. Rosen and G. M. Buccolo, "Perspectives on worldwide spaceborne radar programs," *IEEE Aerospace Conference*, Big Sky, MT, USA, Mar 2007.
- [21] A. M. Walton and M. R. Brown, "Space based radar tracking filter," *IEE Colloquium on Algorithms for Target Tracking*, Savoy Place, London, UK, May 16 1995.
- [22] E. A. Wan and R. van der Merwe, "The unscented Kalman filter for nonlinear estimation," *IEEE Symposium on Adaptive Systems for Signal Processing, Communications and Control*, Lake Louise, Alberta, Canada, Oct 2000.